ELSEVIER

Journal of Structural Geology 29 (2007) 1315–1326

JOURNAL OF STRUCTURAL GEOLOGY

www.elsevier.com/locate/jsg

Rock deformation processes in the Karakoram fault zone, Eastern Karakoram, Ladakh, NW India

E.H. Rutter [a,*], D.R. Faulkner [a,1], K.H. Brodie [a], R.J. Phillips [b,2], M.P. Searle [b]

[a] University of Manchester, School of Earth, Atmospheric and Environmental Sciences, Manchester, M13 9PL, UK
[b] Department of Earth Sciences, University of Oxford, Parks Road, Oxford, OX1 3PR, UK

Received 11 September 2006; received in revised form 29 April 2007; accepted 9 May 2007
Available online 21 May 2007

Abstract

The Karakoram fault shows a full range of fault rocks from ductile (deformation by intracrystalline plasticity) mylonites to low temperature brittle fault rocks along the trace of the fault in the Eastern Karakoram, Ladakh, NW India. The Karakoram fault is a prominent feature on satellite images and has estimated long-term average slip rates between 3 and 11 mm/year, based on U-Pb geochronology of mapped offset markers, notably mid-Miocene leucogranites. Mylonitic marbles, superimposed by cataclastic deformation and clay-bearing fault gouges and late fracturing were found on a presently active strand of the fault, and testify to progressive deformation from plastic through brittle deformation during unroofing and cooling. From microstructural analysis we confirmed the right-lateral strike slip character of the fault, estimated peak differential stresses of ca. 200 MPa at the transition from plastic to brittle deformation, and found microstructural features to be consistent with inferences from the extrapolation of deformation behaviour from experimental rock deformation studies. Implied long-term averaged slip rates from microstructural constraints were found to be broadly consistent with estimates from geochronologic and geodetic studies.

Keywords: Karakoram; Tibet; Faulting; Brittle and plastic deformation; Tectonics

1. Introduction

The 800 km long Karakoram fault zone bounds the southwestern margin of the Tibetan Plateau (Fig. 1). It forms part of a fault network north of the main Himalayan chain that has developed in response to the northward motion of India into Asia. The importance of the fault in Asian tectonics has been highlighted by recent discussion debating the extent to which the Karakoram fault has accommodated India–Asia convergence (Searle, 1996; Searle et al., 1998; Phillips et al., 2004; Searle and Phillips, 2004, 2007; Lacassin et al., 2004a,b; Jade et al., 2004). Observations of the patterns of faulting led several authors to suggest that the Tibetan plateau had been extruded to the east via large movements on the 2500 km long sinistral Altyn Tagh fault, to the north of Tibet, and the dextral Karakoram fault to the southwest (Molnar and Tapponnier, 1975; Peltzer et al., 1989; Meyer et al., 1996; Lacassin et al., 2004a,b) (Fig. 1). Recent work, however, has established that offsets across the Karakoram fault are on the order of only 40–150 km, implying that only a limited amount of extrusion was possible (Searle et al., 1998; Phillips et al., 2004; Searle and Phillips, 2004).

In the Eastern Karakoram, Ladakh, the Karakoram fault splays into two parallel strands, the main Tangtse fault to the SW and the subsidiary Pangong strand to the NE (Fig. 2). The Tangtse fault divides the pre-collisional Ladakh granitoids and Khardung calc-alkaline volcanic rocks to the SW from the metamorphic and magmatic rocks of the Karakoram to the NE, whereas the Pangong fault cuts solely

* Corresponding author. Tel.: +44 161 275 3945; fax: +44 161 275 3947.
E-mail address: e.rutter@manchester.ac.uk (E.H. Rutter).
[1] Present address: University of Liverpool, Earth and Ocean Sciences, Liverpool, L69 3GP, UK.
[2] Present address: CASP, Department of Earth Sciences, University of Cambridge, 181a Huntingdon Road, Cambridge, CB3 0DH, UK.

0191-8141/$ - see front matter © 2007 Elsevier Ltd. All rights reserved.
doi:10.1016/j.jsg.2007.05.001

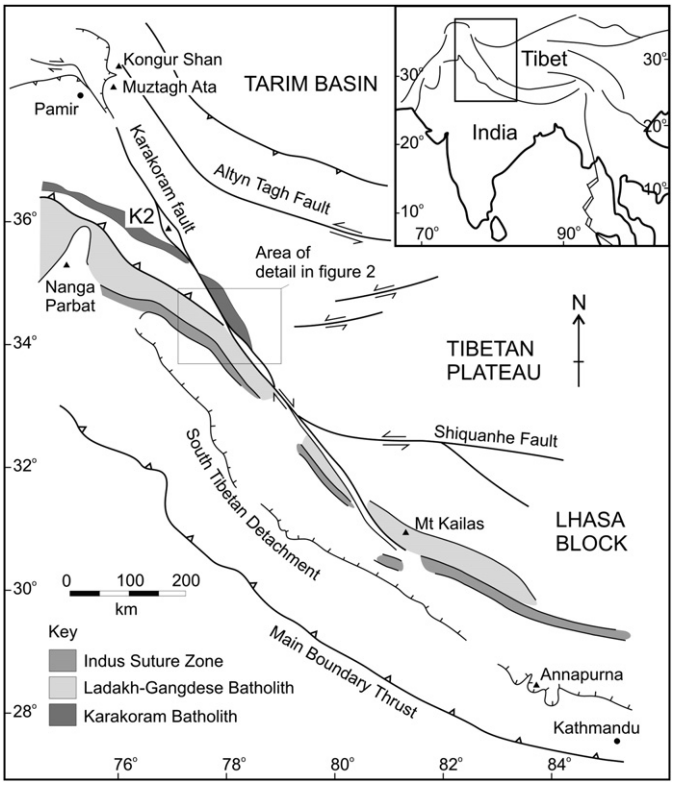

Fig. 1. Regional location map showing the full ~800 km extent of the Karakoram fault and its relation to selected Himalayan features. The central portion of the fault where the current study took place is highlighted and shown in Fig. 2.

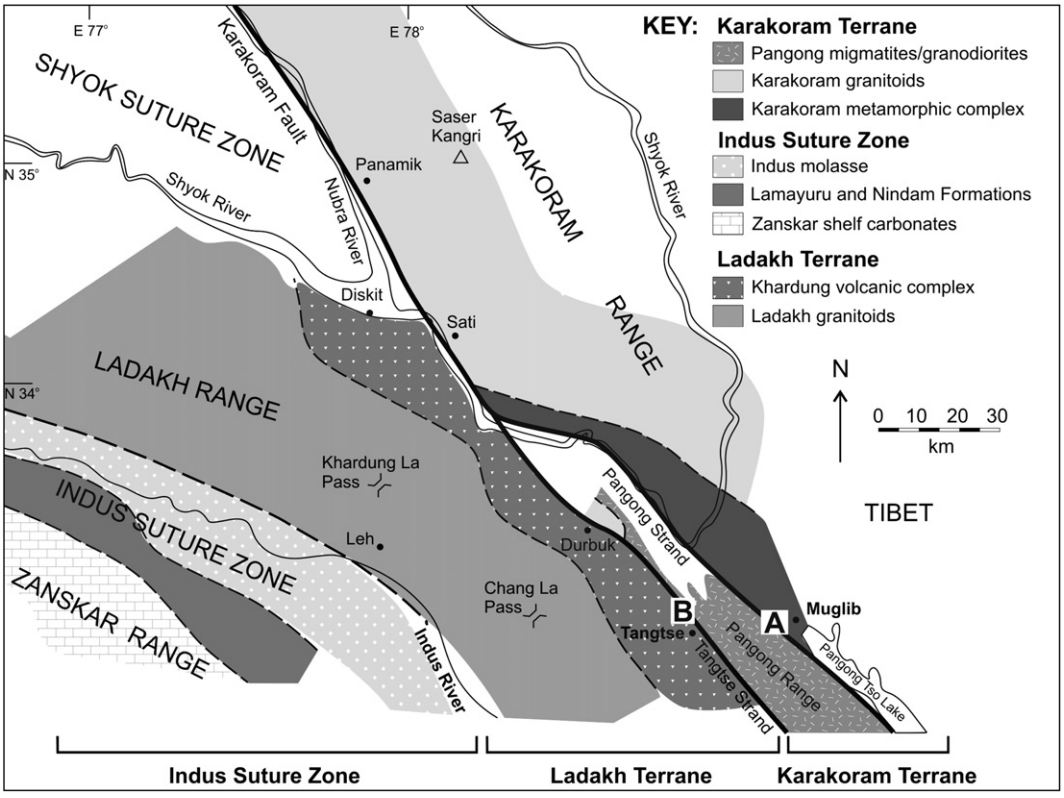

Fig. 2. The central portion of the Karakoram fault highlighting the areas studied. (A) Muglib (Fig. 3); (B) Tangtse gompa (Fig. 6). The regional geology is taken from maps of Searle et al. (1998) and Phillips et al. (2004).

through rocks of the Karakoram terrane. This segment of the Karakoram fault, where the present study is focused, is particularly important because the fault cuts through middle and deep crustal rocks that are not seen along most Tibetan strike-slip faults.

Slip rates estimated at various points along the Karakoram fault appear to show a spatial and secular variation (Chevalier et al., 2005a). The fault zone defines a major topographic feature and evidence for continued activity through to the present day has been reported. Present-day rates based on interferometric synthetic aperture radar (InSAR) analyses show an upper limit of 3 mm/year (Wright et al., 2004), consistent with geodetic rates derived from GPS (Jade et al., 2004). At the million year time scale, Quaternary slip rates along the Pangong branch of the fault were estimated at 4 ± 1 mm/year based on offsets of debris flows dated at 11–14 ka using cosmogenic isotopes (Brown et al., 2002). Chevalier et al. (2005a) used similar dating methods on offset glacial deposits along the Karakoram fault in SW Tibet to propose a slip rate of 10.7 ± 0.7 mm/year, although Brown et al. (2005) questioned the selectivity of age data from a wide scatter of ages from individual clasts (Reply to comment: Chevalier et al., 2005b). Coupled with a lack of historical and recorded seismicity along the fault, these data suggest low seismicity and long earthquake recurrence intervals.

Long-term averaged slip rates have been derived from U-Pb dating of offset leucogranites along the Karakoram fault (Searle et al., 1998; Phillips et al., 2004). Since these 15 Ma leucogranites show low-temperature dextral shearing fabrics superimposed on the igneous texture, the U-Pb ages must provide a maximum age of initiation of the fault (Phillips et al., 2004; Searle and Phillips, 2004).

Most exposures of the deformed rocks of the Karakoram fault zone display evidence of high temperature plastic deformation in silicic rocks, such as metagranitoids. Continuous or episodic movement extending to the present day, as indicated by the observations recorded (above) of Quaternary offsets and radar interferometry, implies that rocks originally sheared deep in the crust must locally have been overprinted by fault rocks developed under progressively shallower crustal conditions as erosion has occurred. Such localities have proved hard to find because so much of the fault zone is buried beneath superficial fluvioglacial and slope deposits. This paper describes the deformed rocks at one such locality. We attempt to infer from microstructural observations the succession of stress/temperature/depth conditions under which they developed, and the implications from these observations for the time-averaged slip rate.

Towards the southeastern part of the region shown in Fig. 2, the fault bifurcates into the Pangong strand to the northeast and the Tangtse strand to the southwest. Exposures of both strands of the fault were studied, at Muglib (N 34° 00′ 55″, E 78° 17′ 03″) and at Tangtse (N 34° 1′ 12″, E 78° 11′ 15″), at either end of the Tangtse gorge, which cuts across the strike of the fault (A to B on Fig. 2). In places where the fault rock exposure was suitable, detailed fault mapping on the scale of 1:3000 was conducted.

2. Deformation in the Pangong fault strand near Muglib

2.1. The Muglib locality

The Muglib locality (Fig. 3) comprises a stretch of exposure some 200 m long and up to 70 m wide, dominantly of calcite marble of the Pangong metamorphic complex that forms the mountains lying to the NE of Muglib. The tract has fortuitously had the cover of glacial debris removed by slope failure and erosion on the outer arc of a river bend. The mountains to the SW are dominated by Late Cretaceous granodiorites and migmatitic gneisses, and mid-Miocene leucogranites and migmatitic leucosomes of the Pangong range, which lies between the two main fault strands (Phillips, 2004; Phillips et al., 2004). Hillwash boulders on the exposure are dominated by these rocks, and the contact between these and the metamorphic rocks seen in the Muglib exposure must lie beneath the debris cover to the south west.

At Muglib, the fault-rock exposure is partitioned into three segments by two fault strands (Fig. 3). The southwestern segment comprises a well-foliated calcite mylonite (40 μm grain size), bearing a thin (1 m wide) layer of biotite-plagioclase schist. In these rocks the grain shape foliation is parallel to the fault trace and dips moderately SW. The other fault segments comprise a coarser calcite marble (200–500 μm grain size) that is heavily fragmented (Fig. 4) with a weakly defined, E-W striking foliation that probably corresponds to thin (1 mm) bands of cataclasite. The fragmented marble fault segments are split by a fault-zone, a few metres thick, consisting of clay-bearing fault gouge. The microstructures within each of the marble segments, and within the clay-bearing fault gouge, reveal different parts of the history of fault movement during progressive unroofing through erosion. Ultra-thin, double polished thin sections were prepared from all carbonate samples. Microstructural characteristics of rocks from this locality are summarized in Table 1 and described below.

2.2. The clay-bearing fault gouge at Muglib

The fault gouges were sampled (locations are indicated in Fig. 3) and their mineralogy was determined by X-ray diffraction (XRD) and differential scanning calorimetry (DSC). The combination of these techniques is particularly useful in identifying clay phases, as these minerals often have overlapping peaks with higher temperature phyllosilicates in the XRD trace. DSC provides information on the dehydration temperatures of the constituent minerals and hence provides information on the proportions of clay phases present. Table 2 shows the results of the XRD and DSC analyses on the samples collected, with the mineralogy for each identified.

Although the chlorite in the fault gouge may be derived from mechanical breakdown of the protolith, it is likely that the illite phase is authigenic, produced during shearing. To estimate metamorphic conditions during shearing the Kübler index for the illite (peak width at half-height for the first basal reflection) was estimated from centrifuged fine-grained concentrates. The value obtained ($2\theta = 2.2 \pm 0.1°$) corresponds

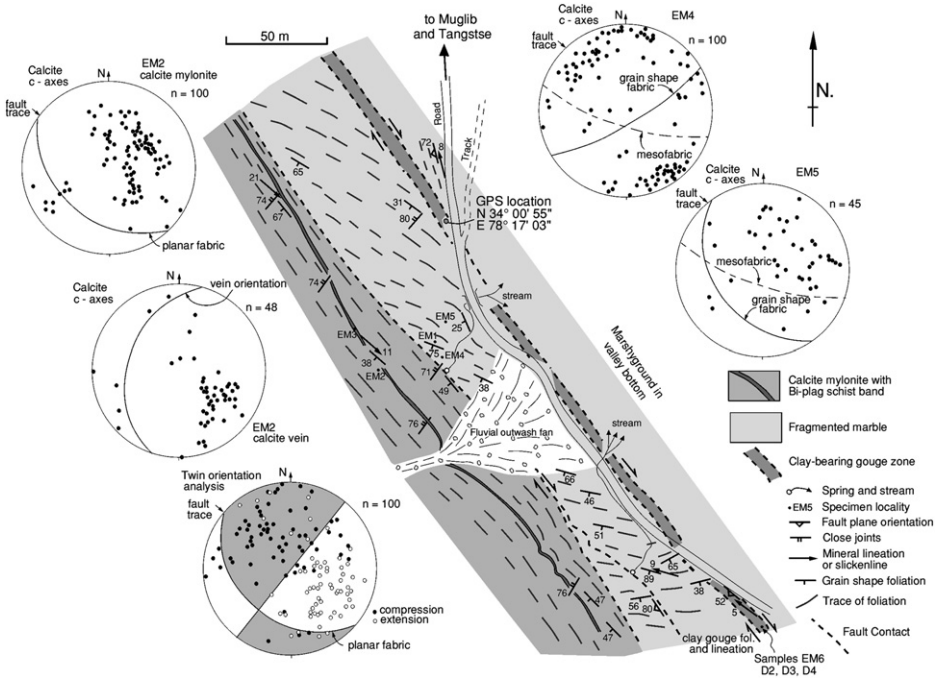

Fig. 3. Muglib fault locality map. Equal area, lower hemisphere projections are shown for marble specimens EM2 (calcite mylonite on the SW side of the exposure) and EM4 and EM5 in the tract of fragmented marbles. For EM2, *c*-axes orientations are shown for the mylonitic matrix and for a cross-fabric calcite vein. The 'beach-ball' diagram (lower left) shows relative extensional axes (open circles) and compressional axes (closed circles) inferred from calcite twinning using the Turner (1953) dynamic analysis technique. The result is consistent with the SW-dipping attitude of the shear zone and a right-lateral movement sense. Plots for EM4 and EM5 *c*-axes are concentrated normal to the grain shape fabric plane but that this is variously reoriented by the fragmentation process. The right-lateral, strike-slip fault movement vector for the clay-bearing fault gouge (SE extremity of map) was determined from the 'P' foliation and 'R_1' Riedel shears. *n* indicates number of data.

to the anchizone to epizone transition (Ji and Browne, 2000). This is tentatively taken to correspond to about 300 °C, whilst bearing in mind that factors other than peak temperature attained can affect peak width (such as time at temperature and the effects of shearing, which would have continued to affect the gouge during continued cooling).

The clay-bearing fault gouges (represented by samples D2, D3 and D4 on Fig. 3) displayed systematic microstructures (Fig. 4b), with P foliations and R_1 Riedel shears visible (Rutter et al., 1986). The geometry of these fabrics indicated a right-lateral, strike-slip sense of shear. These planar features were measured in the field and a sub-horizontal movement vector for the gouge band was constructed from the normal to the intersection of the P foliation and the R_1 Riedel shears, in the acute bisecting plane of these fabrics.

2.3. The calcite mylonite strand at Muglib

The calcite mylonite consists of nearly equigranular, ultra-fine-grained calcite with a small number of rounded porphyroclasts remaining from a coarser-grained protolith. Its microstructure is illustrated in Fig. 4c. Mean planar grain size (38 ± 1.4 μm) and shape preferred orientation was measured automatically from digital maps of the grain boundaries for several hundred grains in sections cut normal to foliation and parallel to lineation, following the methodology of Rutter et al. (1994) and Rutter (1995). Shape preferred orientation of the recrystallized matrix is weak (shape factor = 1.4 using the enhanced-normalized centre-to-centre method; Erslev and Ge, 1990). Textural characteristics of all the marble samples from Muglib are summarized in Table 2.

In thin section the calcite mylonite shows deformation twin lamellae to be present only in the coarser grains. The mylonitic texture was cut at a high angle to the foliation by occasional hydrothermal calcite veins containing grains of various sizes, bearing thin, straight twin lamellae (Fig. 4d). Preservation of the high cross-cutting angle shows that the veins and hence twins formed after mylonitization. Twin lamellae preferred orientation (Fig. 3) and twinning incidence as a function of grain size in calcite (Fig. 5) potentially carry information about the magnitude and orientation of the stress field that produced the twinning (Turner, 1953; Rowe and Rutter, 1990), provided it is imposed after the crystallographic fabric developed (i.e. is not related to the formation of that fabric) and provided there is a sufficient spread of crystallographic orientations in the parent calcite grains. We measured the crystallographic orientation of about 100 calcite grains in the mylonite and in one of the cross-cutting calcite veins using universal stage optical microscopy (Fig. 3). A crystallographic preferred orientation of *c*-axes is developed normal to the mesoscopic foliation defined by grain shape and orientation of occasional mica grains. This is a common fabric type for calcite mylonites deformed to high strains in shear (e.g. Casey et al., 1998; Pieri et al., 2001a,b) but also for uniaxial flattening (Rutter et al., 1994). The calcite grains in the vein show a preferred orientation of *c*-axes normal to the vein wall

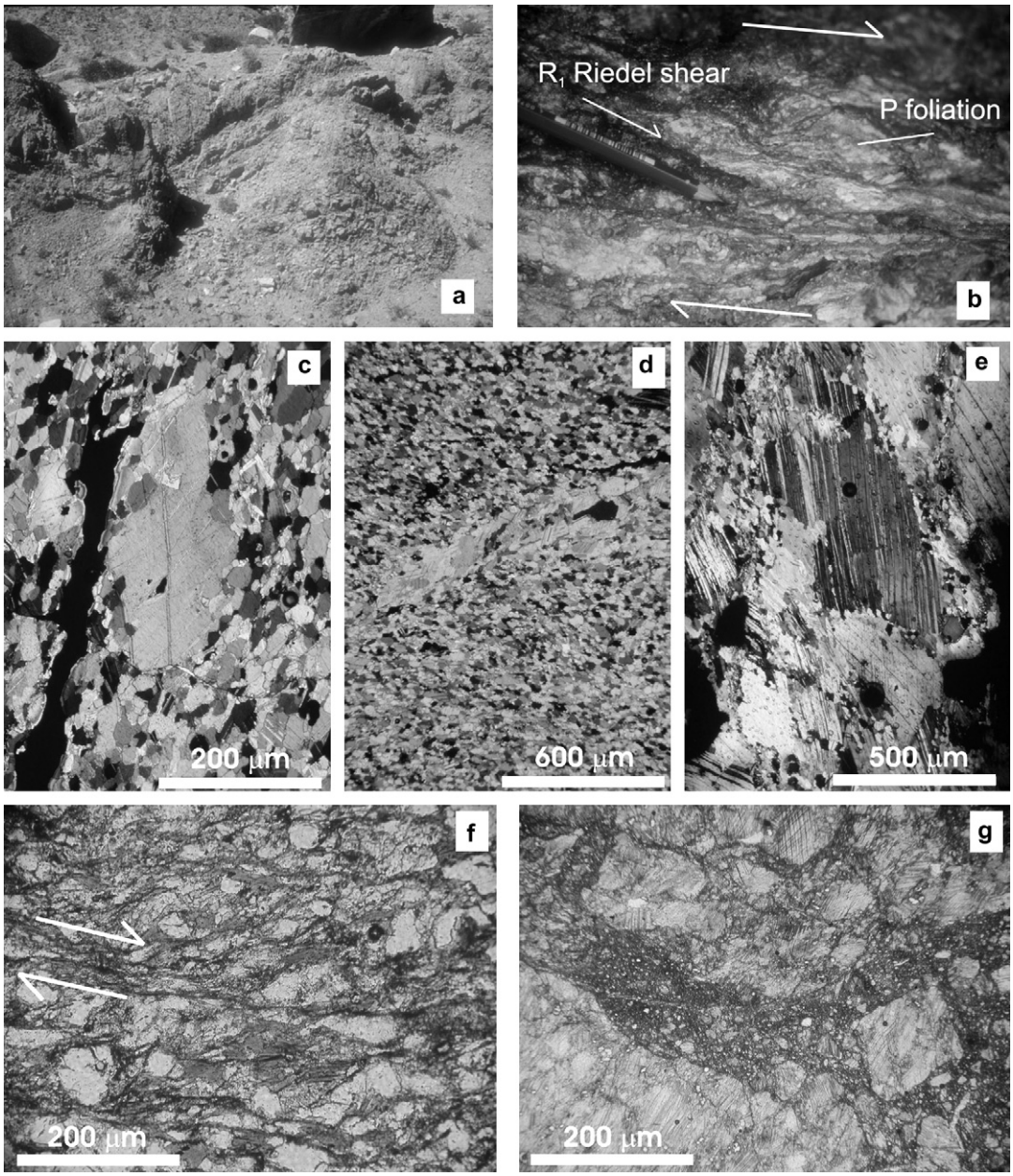

Fig. 4. Structures and microstructures at the Muglib locality (Fig. 3 for specimen locations). (a) Intensely mesofractured marbles in the field (width of photo 4 m, view direction 235°). (b) Field photo of the typical microstructure of the clay-bearing fault gouge (pencil for scale, view direction 50/235). (c) Calcite mylonite microstructure (specimen EM2, XP) with porphyroclast showing subgrains and migration recrystallization reducing the grain size. There is a weak shape fabric in the new grains. (d) Lower magnification image of EM2 (XP) showing the weak grain shape fabric crosscut by a later vein of coarser, twinned calcite crystals (Fig. 3 for relative orientations). (e) Photomicrograph of specimen EM4 (XP) showing host grains with migration recrystallization to smaller grains around host grain boundaries. Large grains are twinned with small amounts of twin-boundary migration. (f) Photomicrograph of the biotite-plagioclase-quartz schist (specimen EM3, PPL) with right lateral shear bands (example indicated) in which brittle fragmentation of feldspar grains has occurred, superimposed on earlier asymmetric biotite growths on plagioclase also indicating right-lateral shear. (g) Micrograph (PPL) of the fragmented but cohesive marble (specimen EM4) with cataclastic fragmentation superimposed on the partially recrystallized and twinned fabric shown in (e). PPL, plane-polarized light; XP, crossed-polars.

(Fig. 3), and this is likely to have been produced by oriented growth of calcite within the vein.

It seems likely that twinning of the coarser grains in the mylonite and in the vein calcite was produced after the mylonitic recrystallization and grain refinement and hence can be used in the Turner (1953) method for the inference of palaeostress orientations. Because deformation twinning can only occur for a sense of shear resolved along the twin plane that displaces the upper layers of the crystal towards the *c*-axis (+ve shear sense), the orientations of relative extension and compression axes can be inferred. These are plotted for the twinned grains in the calcite mylonite in Fig. 3. The data are presented in a manner analogous to the 'beach-ball' diagrams widely used to present data on first-motions from earthquakes and from which shear sense on the operative fault can be inferred. The data show that the twinning behaviour is most

Table 1
Microstructural characteristics of samples collected at the Muglib locality

Sample no.	Grain sizes (μm)			Temperature (°C)	Stress (recryst g.s.) (MPa)	Stress (twin incid.) (MPa)
	Host grains	Recryst	All			
EM1	240 ± 11	40 ± 9	48 ± 10	310 ± 20	98 ± 35	210 ± 30
EM5	430 ± 24	119 ± 20	135 ± 28	375 ± 20	40 ± 20	160 ± 30
EM4	167 ± 12	32 ± 5	48 ± 12	300 ± 20	110 ± 40	250 ± 30
EM2	–	–	38 ± 3	–	102 ± 40	220 ± 30
EM7	370 ± 32	–	–	365 + 125/–25	–	–
P144	560 ± 25	–	–	395 + 125/–25	–	–
P122	1100 ± 147	–	–	480 + 130/–30	–	–
EM3 (mineral assemblage)	–	–	–	460 ± 92	–	–

Metamorphic temperatures are based on host grain size and the temperature/grain size relations observed on Naxos Island (Covey Crump and Rutter, 1989), except for EM3 where temperature is based on mineral assemblage. Stresses from recrystallized grain sizes are inferred to apply to a maximum of the temperature shown, and a minimum of 300 °C, below which brittle deformation begins to supervene. Stresses from twinning incidence are expected to correspond to the maximum on the strength/depth profile.

consistent with right-lateral transpressional displacement on a moderately SW-dipping fault plane. This is consistent with the measured orientation of fault planes within the main fault zone, the orientation of the mylonitic foliation, mineral elongation lineations in the mylonite and occasional asymmetric calcite porphyroclasts.

Planar grain size distribution was also measured for the calcite mylonite (Table 1) from tracings of grain boundaries made from thin sections using the computer program GRAINS (Rutter et al., 1994). Recrystallized grain size can be used to estimate differential stress operative during recrystallization (Rutter, 1995; Table 1).

Within the calcite mylonite is a layer of biotite-plagioclase schist, parallel to the mylonitic foliation and about 1 m thick (Fig. 3). The schist contains Ca-plagioclase (An_{42}) and biotite ($K_{0.92}Na_{0.01}Fe_{1.22}Mg_{1.17}Ti_{0.11}Mn_{0.02}Al_{1.51}Si_{2.82}O_{10}(OH)_2$), but also hornblendic amphibole, quartz, clinozoisite ($Ca_{1.99}Fe^{3+}_{0.46}Al_{2.52}Si_{3.01}O_{12}OH$), calcite, alkali feldspar and accessory apatite. The amphibole grains show some zoning with cores of ferroan pargasitic hornblende ($K_{0.28}Na_{0.36}Ca_{1.93}Mn_{0.06}Fe_{2.24}Mg_{2.11}Ti_{0.11}Al_{2.13}Si_{6.47}O_{22}(OH)_2$) and rims of magnesio-hornblende ($K_{0.14}Na_{0.22}Ca_{1.95}Mn_{0.06}Fe_{2.10}Mg_{2.45}Ti_{0.06}Al_{1.30}Si_{7.08}O_{22}(OH)_2$). The rock displays a schistosity defined by the alignment of biotite, often forming asymmetric tails on plagioclase grains, and possesses a marked horizontal mineral stretching lineation, parallel to that in the calcite mylonite. From this fabric a right-lateral, strike-slip shear sense can be inferred (Fig. 4f). The rock is cut by later brittle shear bands (micro-shear zones slightly oblique to the main foliation), indicating same direction and sense of shear as the asymmetric tails on the plagioclase porphyroblasts. These bands contain small fragments of feldspar derived from adjacent grains (Fig. 4f), and their formation does not appear to have introduced any retrogressive alteration of the mineral paragenesis. Calculations of the bulk composition of the rock indicate SiO_2 of approximately 65–70% (silicic) and Al_2O_3 of ~16% (peraluminous) suggesting that this layer represents a rock of intermediate composition, possibly a dacitic tuff.

Assuming that the above phases were all stable together, THERMOCALC (Holland and Powell, 1998) was used to calculate the P–T conditions of formation. Fig. 5 shows the locus of isobaric invariant points, which equates to the Fe- and Mg-end member discontinuous reactions that are best constrained by the data. The reactions differ by around 20 °C. The average P–T estimated by THERMOCALC based on intersection of the univariant reactions is also shown and is 460 ± 92 °C at 330 ± 230 MPa (error ellipse at 95% confidence shown), and this is taken to correspond to conditions at which synmetamorphic shearing occurred, prior to disruption of the growth fabric by a degree of brittle shearing.

2.4. The fragmented marble strands at Muglib

Compared to the calcite mylonite, the rocks of this tract are much coarser grained (250 μm or greater, Table 1) and are inferred to preserve the same grain size as the metamorphic protolith from which the mylonite was derived. To assess the latter, we examined Karakoram marble samples from three localities at distances from 1 to 6 km from the fault trace, so that the effects of the faulting could be isolated (Table 1). The finest-grained sample (EM7, 3 km NE from fault, grain size 370 ± 32 μm) displays an equigranular foam texture and no deformation twins. Samples P144 (1 km NE from fault), grain size 560 ± 25 μm, some grains twinned) and P122

Table 2
X-ray diffraction and differential scanning calorimetry analyses of the fault gouges collected from the Muglib fault locality

Sample no.	Quartz	Chlorite	Muscovite	Calcite	Dolomite	Microcline	Illite	Saponite	Gypsum
EM6	X		X			X	X	X	
D2	X	X	X	X			X		T
D3	X	X	X	X	X		X		
D4	X	X	X	X	T		X		

An X indicates a major component of the gouge (>10%) where as a T indicates a trace of the mineral within the gouge. Sample localities can be found on Fig. 3.

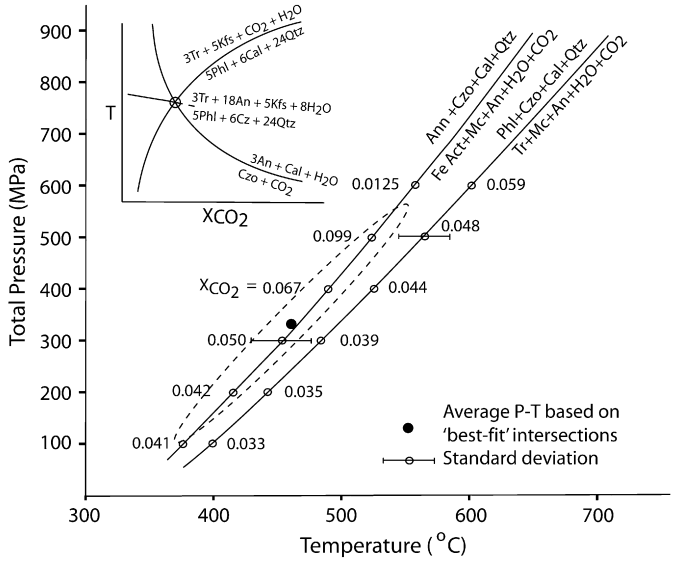

Fig. 5. P–T graph showing the polybaric locus of the invariant points at different constant values of X_{CO2} for the Fe and the Mg end member reactions for the mineral paragenesis of specimen EM3, calculated using THERMOCALC (Holland and Powell, 1998). Inset is a T–X_{CO2} graph at constant P showing schematically the reaction intersections used to determine the invariant points. (Activities of end members calculated at 550 °C, 500 MPa). The standard deviations for temperature estimates are included. Calculations made using the low-Al amphibole analyses are almost identical and have been excluded for clarity. The average P–T calculated from the best-fit intersection of the reactions in this system, using all end members except phlogopite, is also shown, with the error ellipse (dashed line) for 95% confidence. Mineral abbreviations after Kretz (1983).

(6 km NE from fault), grain size 1100 ± 150 μm, all grains twinned) also show equigranular textures but with some evidence of grain boundary mobility. All three samples clearly possessed crystallographic preferred orientation but this was not analyzed. Twin lamellae were generally straight but with evidence of limited twin boundary migration. No sample showed subgrain formation or formation of even incipient tectonic grain refinement by dynamic recrystallization.

The fragmented marbles in the fault zone are similar to the above but also characterized by partial dynamic recrystallization by grain boundary migration around the old grain boundaries but with no discernable subgrain formation (Fig. 4e, also Rutter, 1995 for discussion of the significance of twinning boundary and grain boundary migration recrystallization in calcite rocks), and the parent (larger) grains are twinned with straight twins that display incipient twin boundary migration.

The form of the fragmented marbles in the field is shown in Fig. 4a. Despite their fragmented appearance the rock is generally coherent. Fig. 4g shows the form of fine-grained cemented cataclasite bands that developed between the clasts, which range in size from millimetric to several centimetres across. The coarse host grains in samples from this tract of exposure display a crystallographic preferred orientation of c-axes normal to a weak grain shape fabric that is accentuated by the preferred orientation of twins in the grains (Fig. 4g). It is apparent that cataclastic fragmentation has variously reoriented the clasts so that their (earlier) crystallographic and twinning fabrics cannot be used to infer movement sense and direction in the same way as could be done for the calcite mylonite tract. There is no evidence from microstructural observations that any subsequent plastic deformation of the brittle fragments occurred.

From tracings of host grains and recrystallized grains made from thin sections, separate measurements were made of host and recrystallized grain sizes (Table 1). These data are discussed below.

3. Deformation in the Tangtse fault strand near Tangtse gompa

We observed deformation in the Tangtse fault strand by Tangstse gompa (Buddhist Monastery) (Fig. 6). Here the shearing within the fault zone affects Karakoram granitoids, marble and occasional calc-silicate bands, amphibolite and deformed metapelites. Across the entire width of the fault zone, deformation in all of the lithologies was by intracrystalline plasticity with tectonic grain size reduction and the production of a pervasive foliation. The tectonite fabric in the marbles is affected by to a small degree by superimposed folding of a sense not consistent with the shear sense of the fault zone as a whole. Brittle or other shallow burial deformation features were limited to some widely spaced fractures within the leucogranites (Fig. 6).

The mesoscale deformation fabrics observed, such as rotated porphyroclasts and shear bands at the grain scale, served to confirm dextral strike-slip movements on this portion of the fault. Although we did not make any detailed study of shearing of the granitoids, on the basis of experimental deformation studies it is likely that such deformation, involving tectonic grain size reduction by dynamic recrystallization of quartz, would develop at higher temperature conditions than those that that led to dynamic recrystallization and mylonitization of marbles observed at Muglib. From U-Pb ID-TIMS dating of sheared and unsheared (cross-cutting) dykes at Tangtse, Phillips et al. (2004) concluded that the mylonitization of the granitoids began between 15.68 ± 0.52 Ma and 13.73 ± 0.28 Ma. The latter age is from a leucogranite dyke that cross-cuts the ductile shear fabric but is truncated by a bounding brittle fault. Rolland and Pêcher (2001) proposed that this age dates the thermal peak of amphibolite–granulite metamorphism but our sample clearly cross-cuts and postdates syn-metamorphic fabrics within the host rocks.

4. Discussion

4.1. Significance of different modes of deformation on the Karakoram fault strands at Muglib and Tangtse

Mylonitic leucogranites have previously been recorded along the Karakoram fault (Searle et al., 1998; Phillips et al., 2004). The mineral elongation lineation plunge of 20° NW, observed in mylonitic rocks at Tangtse (Fig. 6), suggest that parts of the fault zone and the country rock to the NE

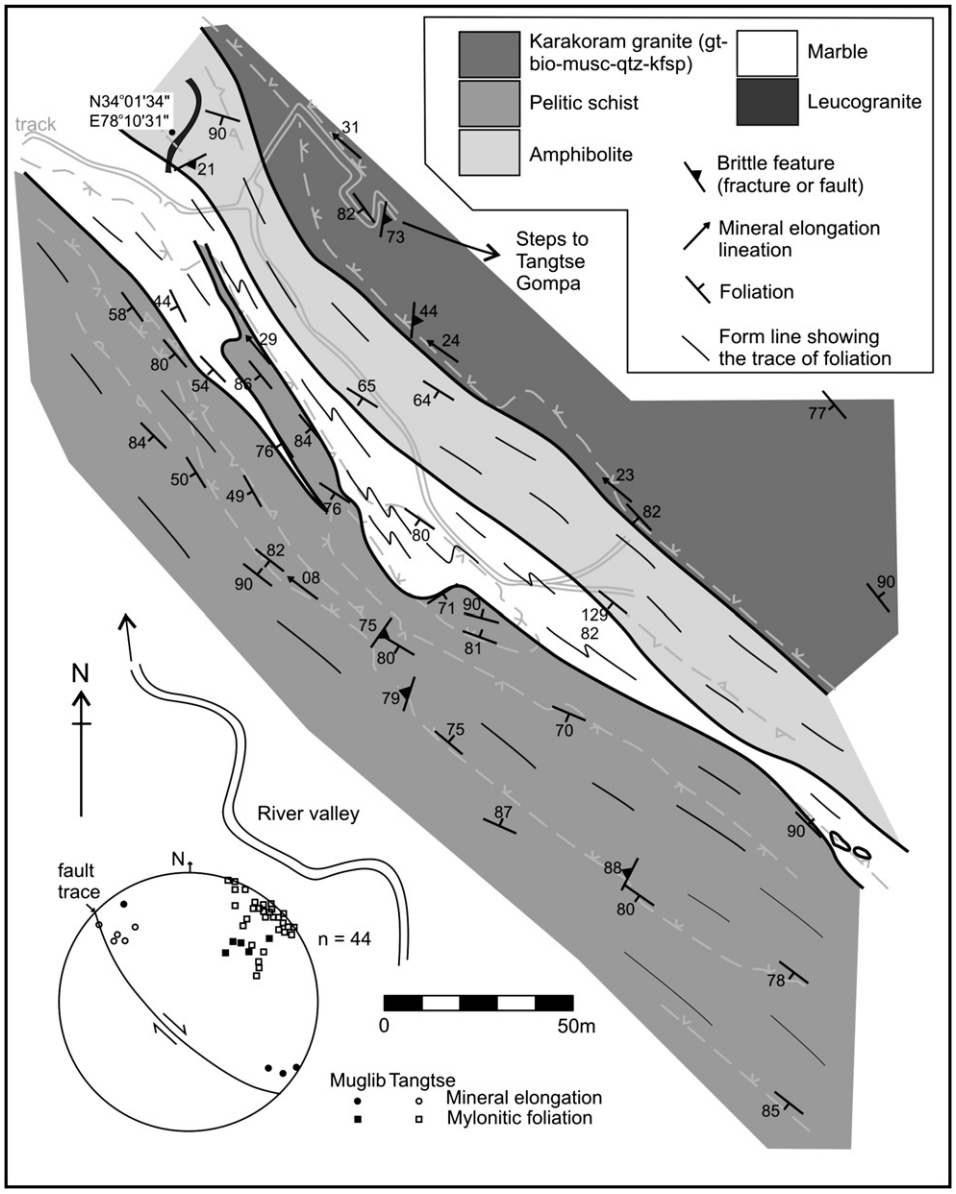

Fig. 6. Map of the Karakoram fault zone (Tangtse strand) at Tangtse gompa (locality B in Fig. 2). Dashed lines with v-ticks indicate topographic breaks of slope. Almost all of the deformation here was by intracrystalline plasticity, and brittle deformation was limited to widely spaced fractures predominantly developed in the granitoids. The leucogranite dyke (upper left) crosscuts the mylonitic fabric and was dated at 13.7 Ma (Phillips et al., 2004), providing a constraint on the minimum age of the mylonitic fabric in the fault zone. Inset equal area lower hemisphere projection shows measurements of the mylonitic foliation at Tangtse and at Muglib, the orientation of mineral stretching lineation in the mylonites and the inferred average orientation of fault planes and movement sense within the Karakoram fault zone.

will have been uplifted as movement progressed, in addition to the general uplift of the region and unroofing by erosion. Thus, a full range of fault rocks, from ductile (deformation by intracrystalline plasticity) mylonites to low temperature brittle fault rocks, should be observed if movement has occurred continuously during exhumation to the surface. Such a range of fault rocks was observed in the Pangong strand of the fault zone at Muglib, but no superimposition of brittle fault rocks on plastically deformed rocks was observed at the Tangtse gompa locality. These observations imply that the more recent movements have been accommodated on the Pangong strand of the fault, rather than the Tangtse strand. The general displacement regime in the fault zone has been inferred to be transpressive (Rolland and Pêcher, 2001), with migmatitic rocks of the Pangong range being uplifted against the SW-dipping Pangong strand of the fault zone (Fig. 2) and the Karakoram metasediments lying to the NE.

4.2. Mixed modes of deformation at the Muglib locality

We have attempted to make a semi-quantitative analysis of the microstructural features observed at Muglib. To provide a framework, Fig. 7 shows an estimate based on laboratory rock mechanics experiments of the expected variation of

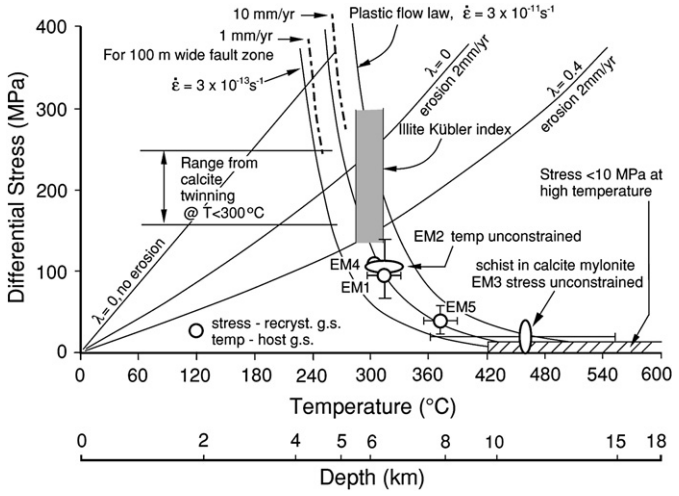

Fig. 7. Variation in differential stress with depth and temperature from laboratory-derived flow laws for calcite and friction coefficients. The temperature and stress estimates from the fault rocks in this study are plotted onto this diagram and uncertainty estimates are given in Table 1. Stress and temperature respectively for specimens EM3 and EM2 are unconstrained, but points (shown as ellipses) are placed according to approximate expected positions. The three curves for the flow stress for calcite plastic deformation are respectively for strain rates of $3 \times 10^{-13}\,s^{-1}$ (leftmost), $3 \times 10^{-12}\,s^{-1}$ and $3 \times 10^{-11}\,s^{-1}$ (rightmost). The intermediate segments of dashed curves are for shear displacement rates indicated for a 100 m wide fault zone transformed into an axisymmetric deformation frame. Sequence of rising stresses with progressive cooling corresponds to the superposition of deformation structures and microstructures observed in the field and in thin section.

differential stress with depth for deformation in a calcite marble-dominated terrain. The horizontal axis shows a linear variation of temperature. In the absence of erosion this axis would also be proportional to depth of burial for a linear geothermal gradient, but in this case we expect rocks to have been deformed under a succession of decreasing pressure/temperature conditions with progressive erosion. We have assumed, for simplicity, a linear erosion rate of 2 mm/year, corresponding to removal of 30 ± km of cover in ca. 15 ± Ma, or since fault movement began (Phillips et al., 2004; Searle and Phillips, 2007). Erosion has the effect of steepening the thermal gradient with depth in the near-surface region and tends to produce nearer-isothermal conditions at depth. This means that the pressure/temperature variations in the later part of the unroofing history are not very sensitive to the initial choice of burial depth. We used a model presented by Reiners and Brandon (2006), modified to a constant boundary condition of 700 °C at 30 km depth at 15 Ma, when leucogranite production would have been occurring. Thus, the non-linear depth scale on Fig. 7 arises from this model.

We presumed a friction coefficient of 0.75 for sliding on near-surface incohesive faults, based on laboratory friction experiments. Thus Fig. 7 shows the variation of differential stress for frictional sliding with depth and temperature for zero pore pressure and for the case of pore pressure = 0.4 of the fault-normal stress ($\lambda = 0.4$). The variation of differential stress with depth in the absence of erosion (corresponding to a geothermal gradient of 23 °C/km) is shown for comparison with the 2 mm/year erosion rate case to demonstrate the effect of taking into account the effect of progressive unroofing. The case of pure strike-slip faulting has been assumed, with maximum and minimum horizontal principal stresses lying equally above and below the intermediate (vertical) principal stress.

The three curves shown for plastic flow of fine-grained marble at different strain rates are based on the grain-size-sensitive flow law of Walker et al. (1990), given by

$$\log\sigma = (\log d\varepsilon/dt - 2.0 + 190000/2.303RT + 1.34\log d)/3.3$$

in which σ is differential stress (MPa), d is grain size (μm), T is absolute temperature, R is the gas constant and $d\varepsilon/dt$ is the strain rate. Deformation according to this flow law is expected to dominate at geologic strain rates under the conditions shown in Fig. 7. It involves a mixture of grain boundary sliding with diffusive and/or intracrystalline plastic accommodation, leading to development of a weak grain shape fabric, a crystallographic preferred orientation and the possibility of cyclic dynamic recrystallization. The microstructural characteristics of the experimentally deformed specimens are identical to those observed in the calcite mylonite at Muglib. This flow law describes axisymmetric flow, but it is easier to convert shear slip rates shown in Fig. 7 into terms of axisymmetric flow rather than the other way around. The width of the Muglib exposure varies up to 70 m and consists entirely of fault rocks, of which only 30 m is plastic mylonite. The fault zone lies within a valley floor, which constrains the fault zone width to no more than 200–300 m. To give an idea of how plastic strain rate corresponds to fault slip rate, for the assumption that plastic shear is concentrated into a zone 100 m wide, slip rates corresponding to 1 mm/year and 10 mm/year are shown on Fig. 7. If the shear is focused into a narrower zone, slip rates will be correspondingly slower and *vice versa*.

Onto this purely theoretical plot we have placed the results of observations at the Muglib locality in terms of stress/temperature conditions:

(a) The grey band is based on the Kübler index for the clay-bearing fault gouge and indicates a metamorphic gradient transitional from anchizone to epizone (temperature 300 ± 30 °C; Ji and Browne, 2000). Even if the illites and chlorites formed at such a temperature, continued shearing at progressively lower temperatures may have mechanically reworked the fabric without reducing crystallinity. The clay-bearing gouge band cuts the fragmented marbles at this locality, which are in turn faulted against the calcite mylonites. This observation constrains the relative ages of these features. We cannot infer directly the temperature/depth conditions of brittle fragmentation of the marble, but to be brittle it is likely to have been cooler than 300 °C (the peak on the differential stress versus depth curve in Fig. 7). Plastic deformation of calcite in nature does occur below 300 °C (e.g. Kennedy and White, 2001) and can accompany or alternate with brittle fracture (e.g. Rowe and Rutter, 1990; Rutter, 1972) as some combination of strain rate or effective pressure is varied, but it

is clear from the microstructure of the fragmented marbles that no further plastic flow followed the fragmentation. The clay-bearing gouge zone cuts the fragmented marbles, implying that brittle deformation in the gouge zone continued long after the crystallinity of the phyllosilicate minerals was developed.

(b) The open circles on Fig. 7 show estimates of flow stress based on the dynamically recrystallized grain size (Table 1) in the fragmented marbles and the grain size of the calcite mylonite, using the migration recrystallized grain size piezometer of Rutter (1995).

(c) The position of the white circles along the temperature axis is constrained by temperature estimates based on measurement of host grain size (i.e. prior to the onset of dynamic recrystallization around the grain boundaries) assuming these marbles behaved like the marbles around the migmatite dome on the Greek island of Naxos (Covey Crump and Rutter, 1989), which show a systematic variation of grain size with palaeotemperature. We recognize that even in relatively pure calcite marbles this correlation is likely not to be unique because grain growth kinetics may be sensitive to trace chemistry and the presence of small, second phase particles and deformation, but it is here taken to provide a first order minimum constraint on the temperature at which the host grain size was equilibrated. Within the Naxos migmatite dome, beneath a low-angle detachment fault, marbles attained temperatures up to 100 °C higher at the same grain size, thus the temperatures reported in Table 1 for samples EM7, P144 and P122 could be systematically low by about that amount. In the Karakoram metamorphic complex the marbles are interlayered with garnet + staurolite-bearing metapelites, that attained peak metamorphic temperatures of amphibolite facies in excess of 500 °C (Phillips, 2004). The large grain sizes attained imply that any operative differential stress during grain growth would have been very small (<10 MPa for a grain size of 400 μm; Rutter, 1995) so that temperature would likely have the dominant effect on grain size. A flow stress level of maximum 10 MPa at temperatures in excess of 400 °C is therefore shown in Fig. 12 as a constraint on the at-depth behaviour.

(d) The mineral assemblage of the biotite-plagioclase schist (EM3) embedded within the calcite mylonite tract also imposes a constraint on the temperature of metamorphic equilibration in the fault zone, whilst right-lateral shear was active, of lowermost amphibolite facies (~460 °C at 330 MPa fluid pressure). This is, however, not necessarily the temperature at which the final grain size of the surrounding calcite mylonite developed, and the depth of burial may have been greater than that corresponding to a total overburden pressure of 330 MPa (about 12 km), according to how much effective confining pressure there was.

(e) Twinning incidence can be used as a basis for estimating *peak* stress to which a zero-porosity calcite rock has been exposed (Rowe and Rutter, 1990). Although carrying an uncertainty of ± 30 MPa even for experimentally deformed samples, this approach remains presently the best constrained method for using twinning to estimate peak stress because it is based on a large number of experiments that show twinning incidence (fraction of grains of a given grain size containing twins) to be insensitive to strain rate and temperature. From both experiments and observations on naturally deformed calcite rocks it is well known that larger grains twin more easily than smaller ones, which means that any palaeopiezometer based on an assumed critical resolved shear stress for twinning that does not recognize grain size sensitivity must be invalid. We measured twinning incidence in five samples from the Muglib locality as a function of grain size (Fig. 5 and Table 1), from which peak differential stress was estimated using the twinning incidence method of Rowe and Rutter (1990). The range of these measurements is indicated on Fig. 8. These peak stresses are likely to have been attained at the depth of the transition from plastic flow to brittle failure and the values obtained are consistent with the predictions from the extrapolation of experimental data for brittle deformation and plastic flow at low to moderate pore fluid pressures. Peak stresses on a fault zone can exceed the far-field average when one takes onto account the effects of inelastic bending around irregularities in the fault surface or at local stress concentrations around asperities.

The above constraints are plotted on Fig. 7 and, when compared with the predictions from experimental data, suggest a mean deformation rate (expressed in terms of axial shortening) of about 10^{-11} s^{-1}. Bearing in mind all the uncertainties present, the sequence of structural and microstructural features developed at Muglib, under conditions of rising stress with progressive unroofing and cooling, seems consistent with the extrapolation of experimental data. The effective width of the Karakoram shear zone at any given time is not known but assuming a 100 m width, the data and model point to a long-term average slip rate on the order of 10 mm/year, or 3 mm/year for a 30 m wide slip zone, when these rocks were at a depth of approximately 6–10 km (3–5 Ma ago).

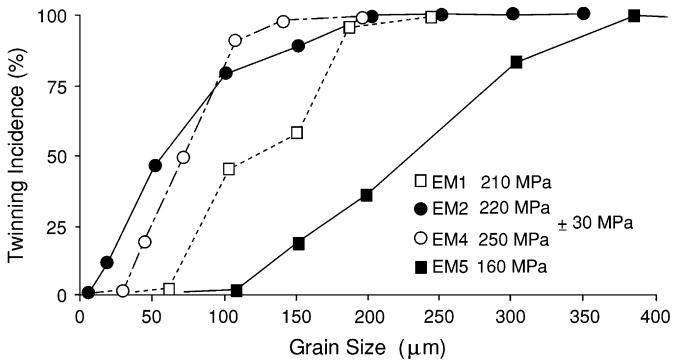

Fig. 8. Plots of twinning incidence (percentage of grains containing twins) versus grain size for four samples collected at the Muglib locality, for the estimation of peak differential stress.

Whilst bearing in mind that the extrapolation of experimental data means that this estimate of strain rate cannot be considered more reliable than within one order of magnitude, it is reasonably consistent with an inferred long-term, time-averaged slip rate of 3–10 mm/year (Phillips et al., 2004) from radiometric dating, 4–11 mm/year for the Quaternary slip rate (Brown et al., 2002; Chevalier et al,, 2005a) from offset morphologic features, and a comparable (but at the lower end of the range) present-day slip rate from GPS/InSAR data (Jade et al., 2004; Wright et al., 2004).

5. Summary and conclusions

The dextral Karakoram fault is a major regional structure that displays between 40 and 150 km offset since initiation at ca. 15 Ma (Searle et al., 1998; Phillips et al., 2004). Long-term average slip rates are around 3–10 mm/year and appear to be consistent with Quaternary rates derived from cosmogenic isotope dating of offset debris flows (Brown et al., 2002), with present-day GPS rates (Jade et al., 2004) and with present-day InSAR data (Wright et al., 2004).

Field studies on the central portion of the Karakoram fault revealed varying degrees of brittle and plastic deformation associated with the movements on the fault. Along the Pangong fault strand, a band of dynamically recrystallized calcite mylonite outcrops, and clay-bearing gouge and cataclastites were found cutting coarse marbles that had suffered partial dynamic recrystallization associated with fault movements. Mineral chemistry, recrystallized grain sizes and calcite twinning were used to help constrain the history of temperature and stress conditions that had affected the fault during progressive unroofing. Inferences from observed microstructural features were found within expected uncertainties to be consistent with a model of stress/temperature conditions based on extrapolation of experimental rock mechanics data, with deformation transitional between cataclastic and intracrystalline plastic processes being attained at about 6 km depth at a differential stress of ca. 200 MPa at about 3 Ma. This would be likely to correspond to the depth limit of seismicity in a carbonate-dominated section. Under these conditions a slip rate of *on the order of* 10 mm/year is inferred, dependent on the assumed width of the active shear zone. The slip rate becomes smaller for a narrower slip zone and *vice versa*. Within the limits of uncertainty of extrapolations of experimental data, this slip rate estimate is consistent with inferences made by other means.

No comparable evidence of relatively shallow/brittle deformation was seen on the Tangtse strand of the fault zone. This observation suggests that the more recent movements (of unknown magnitude) may have occurred preferentially along the Pangong strand of the Karakoram fault.

Acknowledgements

DRF and EHR acknowledge fieldwork support from the Royal Society. RJP and MPS acknowledge support from the Natural Environment Research Council (grant NER/S/A/2000/03515 to RJP and grant NER/K/S/2000/951 to MPS). Fida Hussien of the Rockland Hotel, Leh, is thanked for logistical field support. David Cockram carried out fabric measurements on some of the calcite rocks as part of a student project. Giles Droop is thanked for carrying out the THERMOCALC calculations on the analyses from specimen EM3.

References

Brown, E.T., Bendick, R., Bourlès, D.L., Gaur, V., Molnar, P., Raisbeck, G.M., Yiou, F., 2002. Slip rates on the Karakoram fault, Ladakh, India, determined using cosmic ray exposure dating of debris flows and moraines. Journal of Geophysical Research 107, doi:10.1029/2000JB000100.

Brown, E.T., Molnar, P., Bourlès, D.L., 2005. Comment on "Slip-rate measurements on the Karakorum fault may imply secular variations in fault motion". Science 309, 1326.

Casey, M., Kunze, K., Olgaard, D.L., 1998. Texture of Solnhofen limestone deformed to large strains in torsion. Journal of Structural Geology 20, 255–267.

Chevalier, M.-L., Ryerson, F.J., Tapponnier, P., Finkel, R.C., van der Woerd, J., Haibing, L., Quing, L., 2005a. Slip-rate measurements on the Karakorum fault may imply secular variations in fault motion. Science 307, 411–414.

Chevalier, M.-L., Ryerson, F.J., Tapponnier, P., Finkel, R.C., van der Woerd, J., Haibing, L., Quing, L., 2005b. Response to comment on "Slip-rate measurements on the Karakorum fault may imply secular variations in fault motion". Science 309, 1326.

Covey Crump, S.J., Rutter, E.H., 1989. Thermally induced grain growth of calcite marbles on Naxos Island, Greece. Contributions to Mineralogy and Petrology 101, 69–86.

Erslev, E.A., Ge, H., 1990. Quantitative fabric analysis: least-squares center-to-center and mean object ellipse fabric analysis. Journal of Structural Geology 12, 1047–1059.

Holland, T.J.B., Powell, R., 1998. An internally consistent thermodynamic data set for phases of petrological interest. Journal of Metamorphic Geology, 16309–16343.

Jade, S., Bhatt, B.C., Yang, Z., Bendick, R., Gaur, V.K., Molnar, P., Anand, M.B., Kumar, D., 2004. GPS measurements from the Ladakh Himalaya, India: preliminary tests of plate-like or continuous deformation in Tibet. Geological Society of America Bulletin 116, 1385–1391.

Ji, J., Browne, R.L., 2000. Relationship between illite crystallinity and temperature in active geothermal systems of New Zealand. Clays and Clay Minerals 48, 139–144.

Kennedy, L.A., White, J.C., 2001. Low temperature recrystallization in calcite: mechanisms and consequences. Geology 29, 1027–1030.

Kretz, R., 1983. Symbols for rock-forming minerals. American Mineralogist 68, 277–279.

Lacassin, R., Valli, F., Arnaud, N., Leloup, P.H., Paquette, J.L., Haibang, L., Tapponnier, P., Chevalier, M.L., Guillot, S., Maheo, G., Zhiqin, X., 2004a. Large-scale geometry, offset and kinematic evolution of the Karakorum fault, Tibet. Earth and Planetary Science Letters 219, 255–269.

Lacassin, R., Valli, F., Arnaud, N., Leloup, P.H., Paquette, J.L., Haibang, L., Tapponnier, P., Chevalier, M.L., Guillot, S., Maheo, G., Zhiqin, X., 2004b. Reply to Comment on 'Large-scale geometry, offset and kinematic evolution of the Karakoram fault, Tibet'. Earth and Planetary Science Letters 229, 159–163.

Meyer, B., Tapponnier, P., Gaudemer, Y., Peltzer, G., Shunmin, G., Zhital, C., 1996. Rate of left-lateral movement along the easternmost segment of the Altyn Tagh fault, east of 96E (China). Geophysical Journal International 124, 29–44.

Molnar, P., Tapponnier, P., 1975. Cenozoic tectonics of Asia: effects of a collision. Science 189, 419–426.

Peltzer, G., Tapponnier, P., Armijo, R., 1989. Magnitude of late Quaternary left-lateral displacements along the north edge of Tibet. Science 246, 1285–1289.

Phillips, R.J., 2004. Macro- and micro-structural evolution of the Karakoram fault. Unpublished PhD thesis, University of Oxford, 311 pp.

Phillips, R.J., Parrish, R.R., Searle, M.P., 2004. Age constraints on ductile deformation and long-term slip rates along the Karakoram fault. Ladakh. Earth and Planetary Science Letters 226, 305–319.

Pieri, M., Burlini, L., Kunze, K., Stretton, I., Olgaard, D.L., 2001a. Rheological and microstructural evolution of Carrara marble with high shear strain: results from high temperature torsion experiments. Journal of Structural Geology 23, 1393–1413.

Pieri, M., Kunze, K., Burlini, L., Stretton, I., Olgaard, D.L., Burg, J.-P., Wenk, H.-R., 2001b. Texture development of calcite by deformation and dynamic recrystallization at 1000K during torsion experiments to large strains. Tectonophysics 330, 119–140.

Reiners, P.W., Brandon, M.T., 2006. Using thermochronology to understand erosion. Annual Reviews of Earth and Planetary Science 34, 419–466.

Rolland, Y., Pêcher, A., 2001. The Pangong granulites of the Karakoram Fault (Western Tibet): vertical extrusion within a lithospheric-scale fault? Comptes Rendus de l'Academie des Sciences de Paris 332, 363–370.

Rowe, K.J., Rutter, E.H., 1990. Palaeostress estimation using calcite twinning: experimental calibration and application to nature. Journal of Structural Geology 12, 1–17.

Rutter, E.H., 1972. The influence of interstitial water on the rheological behaviour of calcite rocks. Tectonophysics 14, 13–33.

Rutter, E.H., 1995. Experimental study of the influence of stress, temperature and strain on the dynamic recrystallization of Carrara marble. Journal of Geophysical Research 100, 24651–24663.

Rutter, E.H., Maddock, R.H., Hall, S.H., White, S.H., 1986. Comparative microstructures of natural and experimentally produced clay-bearing fault gouges. Pure and Applied Geophysics 124, 3–30.

Rutter, E.H., Casey, M., Burlini, L., 1994. Preferred crystallographic orientation development during the plastic and superplastic flow of calcite rocks. Journal of Structural Geology 16, 1431–1446.

Searle, M.P., 1996. Geological evidence against large-scale pre-Holocene offsets along the Karakoram fault: implications for the limited extrusion of the Tibetan Plateau. Tectonics 15, 171–186.

Searle, M.P., Phillips, R.J., 2004. A comment on 'Large-scale geometry, offset and kinematic evolution of the Karakoram fault, Tibet' by R. Lacassin et al. Earth and Planetary Science Letters 229, 155–158.

Searle, M.P., Phillips, R.J., 2007. Relationships between right-lateral shear along the Karakoram fault and metamorphism, magmatism, exhumation and uplift: evidence from the K2-Gasherbrum-Pangong ranges, north Pakistan and Ladakh. Journal of the Geological Society of London 164, 439–450.

Searle, M.P., Weinberg, R.F., Dunlap, W.J., 1998. Transpressional tectonics along the Karakoram fault zone, northern Ladakh: constraints on Tibetan extrusion. In: Holdsworth, R.E., Strachan, R.A., Dewey, J.F. (Eds.), Continental Transpressional and Transtensional Tectonics. Special Publication 135. Geological Society of London, London, pp. 307–326.

Turner, F.J., 1953. Nature and dynamic interpretation of twin lamellae calcite of three marbles. American Journal of Science 251, 276–298.

Walker, A.N., Rutter, E.H., Brodie, K.H., 1990. Experimental study of grain-size sensitive flow of synthetic, hot-pressed calcite rocks. In: Knipe, R., Rutter, E. (Eds.), Deformation Mechanisms, Rheology and Tectonics. Special Publication 54. Geological Society, pp. 259–284.

Wright, T.J., Parsons, B., England, P., Fielding, E., 2004. InSAR observations of low slip rates on the major faults of western Tibet. Science 305, 236–239.